catalysts

MDPI

Article

Investigation on the Edge Doping Process of Nitrogen-Doped Carbon Materials by In Situ Pyrolysis Mass Spectrometry and Laser-Induced Acoustic Desorption Mass Spectrometry

Yihuang Jiang [1], Zaifa Shi [1], Qingjie Zeng [1], Jiangle Zhang [1], Zefeng Deng [1], Qiaolin Wang [2,3], Jing Yang [1], Jingxiong Yu [4,*], Zhengbo Qin [2,*] and Zichao Tang [1,*]

[1] State Key Laboratory of Physical Chemistry of Solid Surfaces, College of Chemistry and Chemical Engineering, Xiamen University, Xiamen 361005, China
[2] Anhui Province Key Laboratory of Optoelectric Materials Science and Technology, School of Physics and Electronic Information, Anhui Normal University, Wuhu 241002, China
[3] Key Laboratory of High Power Laser and Physics, Chinese Academy of Sciences, Shanghai 201800, China
[4] Key Laboratory of Interfacial Physics and Technology, Shanghai Institute of Applied Physics, Chinese Academy of Sciences, Shanghai 201800, China
* Correspondence: yujingxiong@sinap.ac.cn (J.Y.); wave0403@163.com (Z.Q.); zctang@xmu.edu.cn (Z.T.)

Abstract: Nitrogen-doped carbon materials demonstrate high performance as electrodes in fuel cells and higher oxygen reduction reactivity than traditional Pt-based electrodes. However, the formation process of nitrogen-doped carbon materials has long been a mystery. In this study, the formation mechanism of nitrogen-doped carbon materials from polyaniline (PANI) pyrolysis was studied by the combination of in situ pyrolysis vacuum ultraviolet photoionization time-of-flight mass spectrometry (Py-VUVPI-TOF MS) and substrate-enhanced, laser-induced acoustic desorption source time-of-flight mass spectrometry (SE-LIAD-TOF MS). The initial pyrolysis species, including free radicals and intermediates, were investigated via in situ Py-VUVPI-TOF MS during the temperature-programmed desorption process (within tens of microseconds). The pyrolysis residues were collected and further investigated via SE-LIAD-TOF MS, revealing the product information of the initial pyrolysis products. The results show that the edge doping of carbon materials depends on free radical reactions rather than the direct substitution of carbon atoms by nitrogen atoms. Meanwhile, pyrrole nitrogen and pyridine nitrogen are formed by the free radical cyclization reaction and the amino aromatization reaction at the initial stage of pyrolysis, while the formation of graphitic nitrogen depends on the further polymerization reaction of pyrrole nitrogen and pyridine nitrogen.

Keywords: nitrogen-doped carbon materials; polyaniline; in situ pyrolysis; vacuum ultraviolet photoionization; laser-induced acoustic desorption

Citation: Jiang, Y.; Shi, Z.; Zeng, Q.; Zhang, J.; Deng, Z.; Wang, Q.; Yang, J.; Yu, J.; Qin, Z.; Tang, Z. Investigation on the Edge Doping Process of Nitrogen-Doped Carbon Materials by In Situ Pyrolysis Mass Spectrometry and Laser-Induced Acoustic Desorption Mass Spectrometry. *Catalysts* **2023**, *13*, 830. https://doi.org/10.3390/catal13050830

Academic Editor: Maurizio Muniz-Miranda

Received: 7 March 2023
Revised: 14 April 2023
Accepted: 19 April 2023
Published: 30 April 2023

1. Introduction

Precious metals (Au, Ag, Pt, etc.) are widely used in catalysis, hydrogen fuel cells, lithium batteries, and other fields due to their unique physical and chemical properties [1–3]. However, the high cost and low reserves of precious metals act as barriers to them being used more commonly. Heteroatom-doped carbon materials (graphene, graphite, porous carbon, etc.) have the dual advantages of excellent physical and chemical properties, and low cost, making them ideal substitutes for precious metals. N-doped carbon graphene has an even better redox performance than traditional Pt-based electrodes when used as fuel cell electrodes [4]. Among the many types of heteroatom-doped (sulfur, nitrogen, boron etc.) carbon materials, nitrogen (N)-doped carbon materials are the ideal candidates to replace precious metals. The atomic radius of nitrogen (0.74 Å) is very close to that of carbon (0.77 Å), and the electronegativity of nitrogen (3.04) is much higher than that of carbon (2.55). Therefore, nitrogen is more easily incorporated into carbon materials

than other heteroatoms, and can significantly optimize the electron distribution of carbon materials [5,6]. In recent years, nitrogen-doped carbon materials have been used in many fields, such as fuel cells, lithium–sulfur batteries, catalysts for oxygen reduction, and electronic devices [7–9]. Unfortunately, the inability to control nitrogen doping and low doping doses is still the main obstacle to further enhancing its performance [5,10].

The nitrogen in N-doped carbon materials mainly exists in the form of pyridine nitrogen, pyrrole nitrogen, graphitic nitrogen, and amino (Figure 1) [11]. The existence, form, and content of doped nitrogen determine the reactivity of nitrogen-doped carbon materials [12,13]. For example, the pseudocapacitance in N-doped carbon materials has been attributed to negatively charged groups at the edge of graphene, such as pyridine, while positively charged groups, such as quaternary N and oxidized N, have no effect on the pseudocapacitance [12,14]. However, there is still no clear explanation of the functional characteristics of nitrogen functional groups in N-doped carbon materials. In the application of N-doped carbon materials for fuel batteries, the functional characteristics of doped nitrogen have been controversial. The functional groups that play a leading role in the redox performance of nitrogen-doped carbon materials (pyridine nitrogen, graphitic nitrogen, synergistic effect of pyridine nitrogen, and graphitic nitrogen) have not yet been determined [6,15–18]. The diversity of nitrogen-containing functional groups in N-doped carbon materials makes it difficult for researchers to accurately determine the properties of different nitrogen-containing functional groups. The controllable synthesis of nitrogen functional groups is the ultimate path to research N-doped carbon materials [10,19]. In principle, it is very difficult to directly replace carbon atoms with nitrogen atoms and the doping process should mainly occur at the edge. However, in the XPS characterization of nitrogen-doped carbon materials, it was found that the content of graphitic nitrogen is not lower than that of pyridine nitrogen and pyrrole nitrogen (at the edge position) [20–23]. Therefore, there are still complex problems and a lack of corresponding mechanisms in the nitrogen doping process.

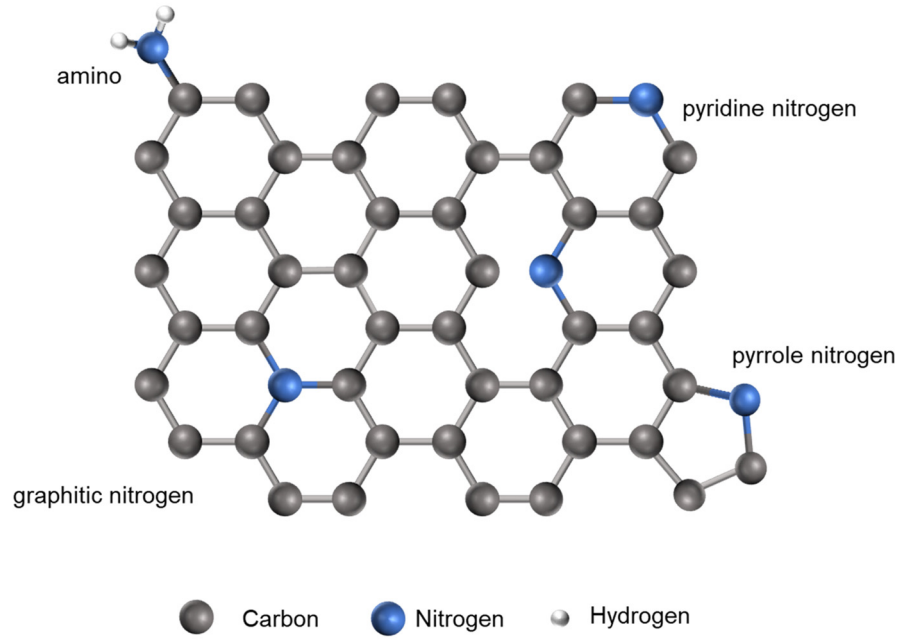

Figure 1. Nitrogen-containing functional groups in N-doped carbon materials.

Because the XPS characteristic peaks corresponding to different nitrogen functional groups are too close, the XPS diagram of N-doped carbon materials often shows a wide peak, which greatly limits the accurate characterization of nitrogen-containing functional groups [16,22,23]. The combination of temperature-programmed desorption and mass spectrometry is an effective means to obtain information of nitrogen atoms located at the

edge in the nitrogen doping process [6,24]. Mass spectrometry technology can provide intuitive feedback on the chemical composition and structural characteristics of compounds through m/z information. Py-VUVPI-TOF MS is an in situ mass spectrometry analysis method developed by the research team, which can obtain initial pyrolysis product information, including information on free radicals. The traditional GC-MS method extensively suppresses the subsequent reactions of the initial pyrolysis products, so Py-VUVPI-TOF MS has great advantages in detecting pyrolysis reactions. Due to its low cost, easy synthesis, and definite structure, polyaniline (PANI) has become one of the precursors which is most commonly used for the synthesis of nitrogen-containing carbon materials [25–27]. In this work, PANI was used as a model compound for the nitrogen-doping process (as both the nitrogen source and the carbon source). The nitrogen in PANI is in the form of a C–N bond, which avoids the misjudgment of the source of the pyrrole nitrogen, pyridine nitrogen, and graphitic nitrogen in the reaction. The pyrolysis process of polyaniline is an ideal model reaction for studying the nitrogen doping process in the pyrolysis process. In situ Py-VUVPI-TOF MS was used to investigate the initial process of nitrogen doping (carried out under vacuum to avoid a secondary reaction) [28,29]. At the same time, SE-LIAD-TOF MS and in situ Py-VUVPI-TOF MS were combined to investigate the intermediate state between the initial reaction products and the final products [30]. Because there was still a small amount of secondary reactions during the Py-VUVPI-TOF MS experiment and the products remained in the instrument, it was necessary to use SE-LIAD-TOF MS to analyze pyrolysis residues without selectivity or fragmentation, and with a high sensitivity to the test substance. By combining two mass spectrometry techniques, the complete conversion process, from the formation of initial pyrolysis products to the final products during the PANI pyrolysis, was comprehensively studied at a molecular level. The resulting information can help researchers better understand the thermal conversion chemical process of nitrogen-containing functional groups, something which has not been reported in previous studies.

2. Results

The initial pyrolysis product information of PANI is shown in Figure S1. The initial products of polyaniline are distributed in the range of m/z 17–600 and contain hundreds of characteristic peaks. Although the PANI pyrolysis mass spectrometry information is relatively complicated, it still follows certain rules. The pyrolysis products of PANI can be roughly divided into three categories: 1. The main pyrolysis products can be classified into seven categories, being three types of polymers ($C_{6n+6}H_{5n+6}N_n$ (polymer-I), $C_{6n+6}H_{5n+7}N_{n+1}$ (polymer-II), and $C_{6n+6}H_{5n+8}N_{n+2}$ (polymer-III)), and four types of nitrogen heteroatom cyclization products ($C_{6n+8}H_{5n+9}N_{n+1}$ (N-cycle-I), $C_{6n+8}H_{5n+9}N_{n+2}$ (N-cycle-II), $C_{6n+9}H_{5n+8}N_{n+2}$ (N-cycle-III), and $C_{6n+9}H_{5n+18}N_{n+2}$ (N-cycle-IV)). The n in the general chemical formula refers to the number of the aniline monomer structure, so the mass spectrum information in the range of $n = 0$ can completely reflect the pyrolysis reactions of PANI (Figure 2); 2. Small molecule products (m/z = 0–78); and 3. free radicals produced during pyrolysis, where the main products are classified according to the structural characteristics in Table S1. Based on pyrolysis product characteristics, the main pyrolysis reactions of PANI can be classified as three basic types: 1. C–N bond cleavage; 2. aromatic ring cleavage (C–C bond cleavage); and 3. an amino-based aromatization reaction. The initial process of the PANI pyrolysis reaction is described in detail, based on the basic reaction type.

The cleavage of the C–N bond in PANI initiates the chain dissociation reaction in the pyrolysis reaction. The spectrum of the related products generated by breaking the C–N bond is shown in Figure S1. The monomers and polymers of aniline are the main products of the destruction of the C–N bonds, and their general chemical formulas are polymer-I, polymer-II, and polymer-III, and the main difference between them is only the number of terminal amino groups. Additionally, PANI mainly forms NH radicals by breaking the C–N bonds on both sides of N. NH radicals (IE = 12.8 eV) and NH_2 radicals

(IE = 11.14 eV) are limited by the ionization energy of the vacuum ultraviolet lamp, which cannot be directly detected [31,32]. Fortunately, N_2H_2 was detected in the in situ pyrolysis experiment (as shown in Figure S2), as it is mainly generated by the NH radical reaction. It has been reported in the literature that the collision reaction of the NH radical to produce N_2H_2 is a barrier-free process [33], so it can be used as an indicator of the generation of NH during the pyrolysis of polyaniline. As an active free radical, NH radicals will react quickly with other molecule pyrolysis products (C_3H_5, C_3H_6, C_4H_8, etc.) to form nitrogen-containing compounds (C_3H_7N, C_4H_4N, C_4H_5N, $C_3H_4N_2$, $C_4H_{13}N_3$, etc.) [34,35]. In addition, compounds with high ionization energy (IE), such as HCN (IE = 13.6 eV), should also be generated at the same time [36].

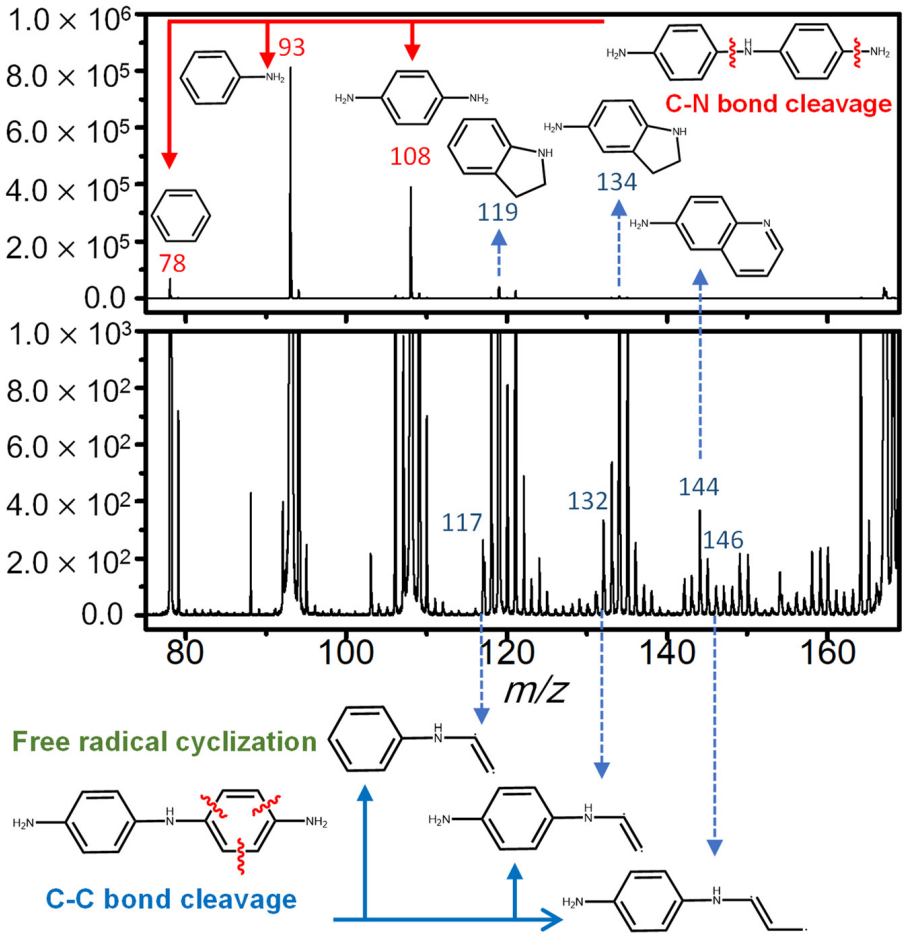

Figure 2. The in situ pyrolysis mass spectrum of PANI, and the dissociation reaction of the C–N bond and benzene ring when $n = 0$ (m/z = 75–170).

Thermal volatilization, covalent bond breakage, and other thermal behaviors during pyrolysis, as well as their rates, are directly affected by the pyrolysis temperature. In experimental in situ Py-VUVPI-TOF MS, the pyrolysis behavior can be accurately described by establishing the functional relationship between ionic strength and temperature. The total ion current (TIC) of PANI is shown in Figure 3a. Similar to derivative thermogravimetric analysis (DTG), the ion current curve of pyrolysis products should conform to normal distribution. The TIC curve of PANI is mainly composed of five characteristic peaks after the peak fitting processing: 1. aniline polymers with a low degree of polymerization in the sample (214 °C and 268 °C); and 2. the main pyrolysis products of PANI (389 °C, 493 °C, and 585 °C).

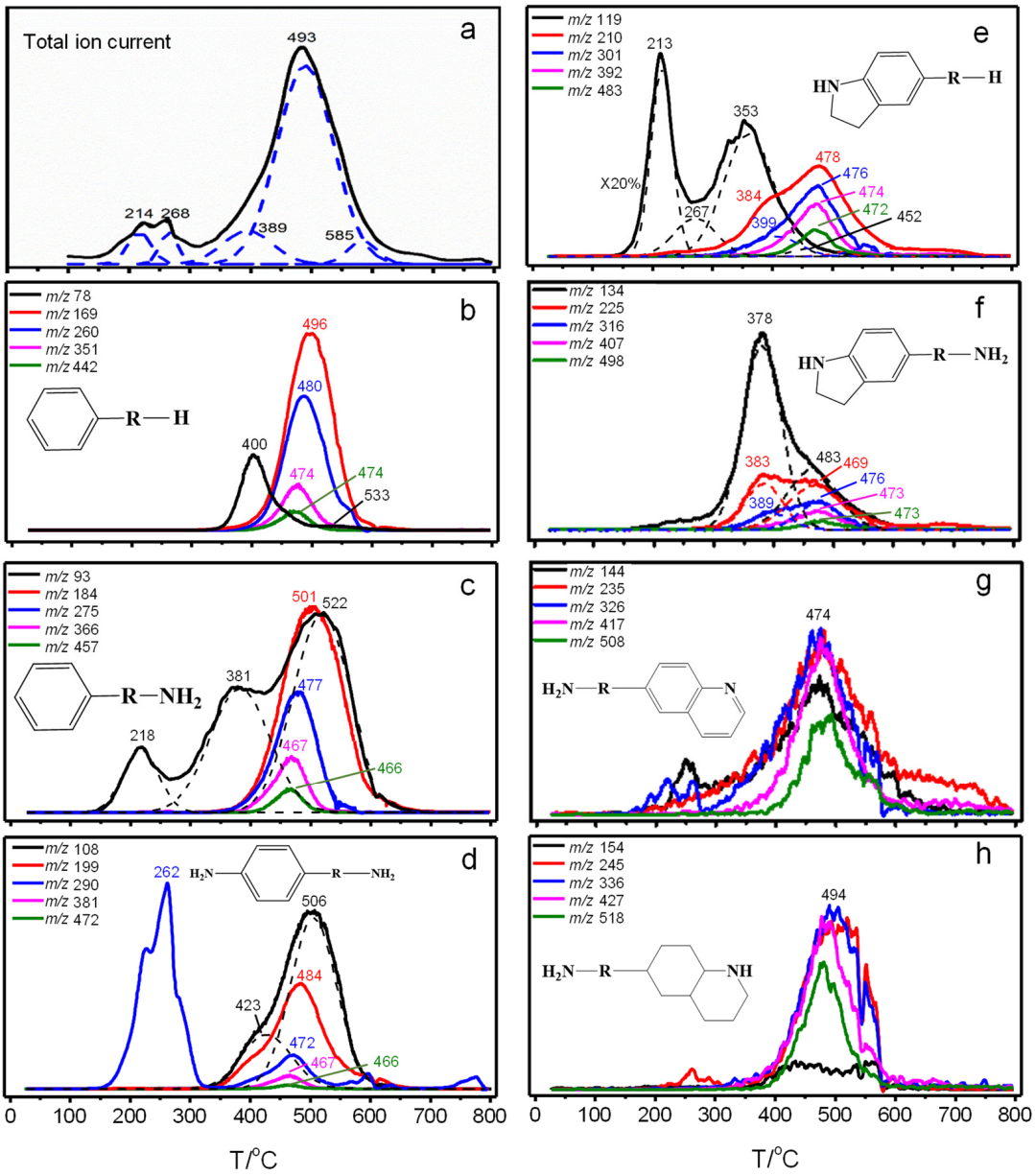

Figure 3. Total ion current (**a**), ion current of polymer-I (**b**), polymer-II (**c**), polymer-III (**d**), N-cycle-I (**e**), N-cycle-II (**f**), N-cycle-III (**g**), N-cycle-IV (**h**) (the R group represents *n* aniline units, *n* in the R group is 0 to 4).

By comparing the ion current of polymer-I (Figure 3b), polymer-II (Figure 3c), and polymer-III (Figure 3d), it is obvious that the C–N bond can be divided into the C–N bond at the end of the polymer and the C–N bond inside the polymer. According to the bond order information of the aniline tetramer (Figure 4), the theoretical calculations show that the C–N bond order at the end of the polymer is stronger than the C–N bond order inside the polymer, indicating that the C–N bond inside the polymer is easier to break. The cleavage of the C–N bond began at about 260 °C and the initial pyrolysis mainly occurred on the weaker C–N bond in the PANI center. Therefore, the pyrolysis products in the temperature range of 260–400 °C are mainly monomer compounds, such as benzene (m/z 78), aniline (m/z 93), and phenylenediamine (m/z 108). When the temperature is higher than 350 °C, the C–N bond near the end of PANI gradually reaches the breaking condition and begins to form polymers of aniline.

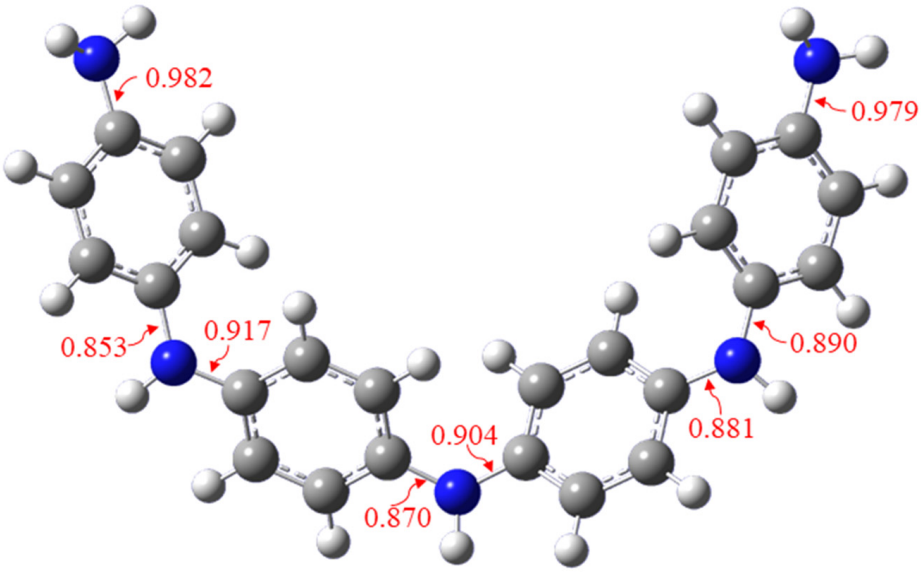

Figure 4. Bond order information of PANI (aniline tetramer): blue represents N, gray represents C, and white represents H.

The cleavage of aromatic bonds In the benzene ring can form C_3H_6, C_4H_8, and other molecular hydrocarbons and free radicals. These small molecular products can form C_3H_7N, C_4H_4N, C_3H_5N, and other nitrogen-containing compounds by containing free radicals such as NH and HCN (Table S1). However, from the bond order information of the benzene ring in PANI (Figure S3) and the small molecule products (m/z = 0–78) with low-intensity peaks in mass spectrometry (Figures S1 and S2), it can be seen that due to the stable structure of the benzene ring, the complete dissociation products of the aromatic ring only account for a small portion of the initial pyrolysis products. The dissociation reactions of the aromatic rings are mainly partial-cracking. When the delocalized π bond of the benzene rings is pyrolyzed, the remaining carbon–nitrogen branches form nitrogen-containing heterocyclic compounds through free radical cyclization reactions (Figure 2). The source of the branched carbon nitrides may be derived from the inherent structure of PANI or the addition reaction of the free radicals. The process of the free radical cyclization reaction is represented by the nitrogen-containing cyclization products at n = 0 (N-cycle-I, N-cycle-II, N-cycle-III, and N-cycle-IV, Figure 2). The free radicals and intermediates in the reaction process can be detected in the mass spectrum. The reaction process should be the conversion of the marginal amino functional groups to pyridine nitrogen and pyrrole nitrogen in the nitrogen doping reaction. Four types of compounds containing the nitrogen heterocyclic structures N-cycle-I, N-cycle-II, N-cycle-III, and N-cycle-IV, are regularly distributed in the initial pyrolysis products of PANI (Figure 2). The ion current information of the N-cycle-I, N-cycle-II, N-cycle-III, and N-cycle-IV (Figure 3e–h), is represented by the monomer (n = 0). For example, according to the peak fitting analysis, all compounds belonging to the N-cycle-I have consistent characteristic pyrolysis peaks (Figure S4). The ion current characteristics of N-cycle-I, N-cycle-II, N-cycle-III, and N-cycle-IV, show that it not only represents some types of compounds, but also contains complex isomers (Figure S5). The possible isomer structures of heterocyclic compounds were optimized by theoretical calculations (Figure S7). It is worth noting that except for a few structures (such as the structural formula given in Table S1), most isomers have the phenomenon of benzene ring distortion. This means that except for a few more stable structures, most of them are unstable and will be further transformed into pyridine, pyrazine, and carbon–nitrogen chain compounds. The formation pathways of the N-cycle-III and N-cycle-IV are more complicated. In addition to the free radical cyclization reactions similar to N-cycle-I and N-cycle-II, they can also be formed by thermochemical conversion of N-cycle-I and N-cycle-II containing pyrrole structures [37]. According to the ion current information of N-cycle-III

and N-cycle-IV, it has at least three isomers, except pyridine compounds, which are easily deduced. The temperature of the characteristic peaks of ion current in N-cycle-III and N-cycle-IV is higher than that in N-cycle-I and N-cycle-II. This phenomenon proves that there is a conversion reaction from pyrrole to pyridine during pyrolysis. And the formation of pyridine nitrogen and pyrrole nitrogen depends on the free radical cyclization reaction of the branched carbon nitrogen functional groups. This means that high temperature conditions provide enough carbon and nitrogen radicals for the subsequent cyclization reactions in the nitrogen doping reactions.

During the pyrolysis process, the combination of free radical rings is not the only way to form nitrogen-containing heterocycles with pyrrole structures. Amino-based aromatization reaction does not involve the cleavage of a C–N bond and a C–C bond (Figure 5). Through the unique mass spectrometry information of aniline polymers (polymer-I, polymer-II, polymer-III), the cyclization phenomenon in the pyrolysis process of PANI can be determined. As shown in Figure 5, with the increase in the polymerization degree (n) of aniline, the degree of unsaturation of the polymer can continue to increase. All the carbons in these polymers are in the aromatic ring, and the cyclization process, as shown by Figure 5, is the only way to increase the degree of unsaturation. The presence of an amino particle is the key to cyclization. We used the B3LYP function and a 6-31G(d) basis set to calculate the enthalpy change of the amino aromatization reaction in Figure 5. At this time, considering the influence of the zero-point energy and temperature effect, we calculated that $\Delta H = -1.49$ Kcal/mol, indicating that this reaction is thermodynamically feasible, which further confirmed the possibility of the amino aromatization reaction. In addition, there were mass spectra peaks with a molecular mass minus one in front of the spectral peaks of all cyclization products. These peaks represent free radicals formed by removing hydrogen atoms from the compound product. Most of the undetermined mass peaks in the pyrolysis products come from the dehydrogenation reaction. The existence of such abundant free radicals in the pyrolysis process of PANI means that the addition reaction of free radicals is inevitable. Since the carbon located at the center of the carbon material has no basis to form free radicals, the nitrogen-containing functional groups can only undergo an addition reaction at the edge of the carbon material. Therefore, the reaction of nitrogen atoms into the structure of the carbon material can only occur at the edges and defects. Alongside that, the sp^3 hybrid orbital of the C–N bond gives the potential to form various spatial structures. With the increase in polymerization, the cyclization of aniline polymers is not only limited to the formation of carbazole-like planar structures, but may also form more complex spatial configurations. In addition, when the polymer terminal contains an amino group (-NH_2), it will increase by a degree of cyclization. The increase in the degree of cyclization can be attributed to the fact that the additional amino groups may not be the residues of the original PANI after pyrolysis, but of the free addition reaction of the benzene ring and the NH radical during the pyrolysis process. Additional amino groups may replace any hydrogen atom in the polymer, resulting in new cyclization methods, such as a phenazine structure. By comparing the ion currents of different cyclization degrees of polymer-I, it was concluded that the cyclization reaction began at about 500 °C, and the cyclization degree of aniline polymer was positively correlated with temperature (Figure S6).

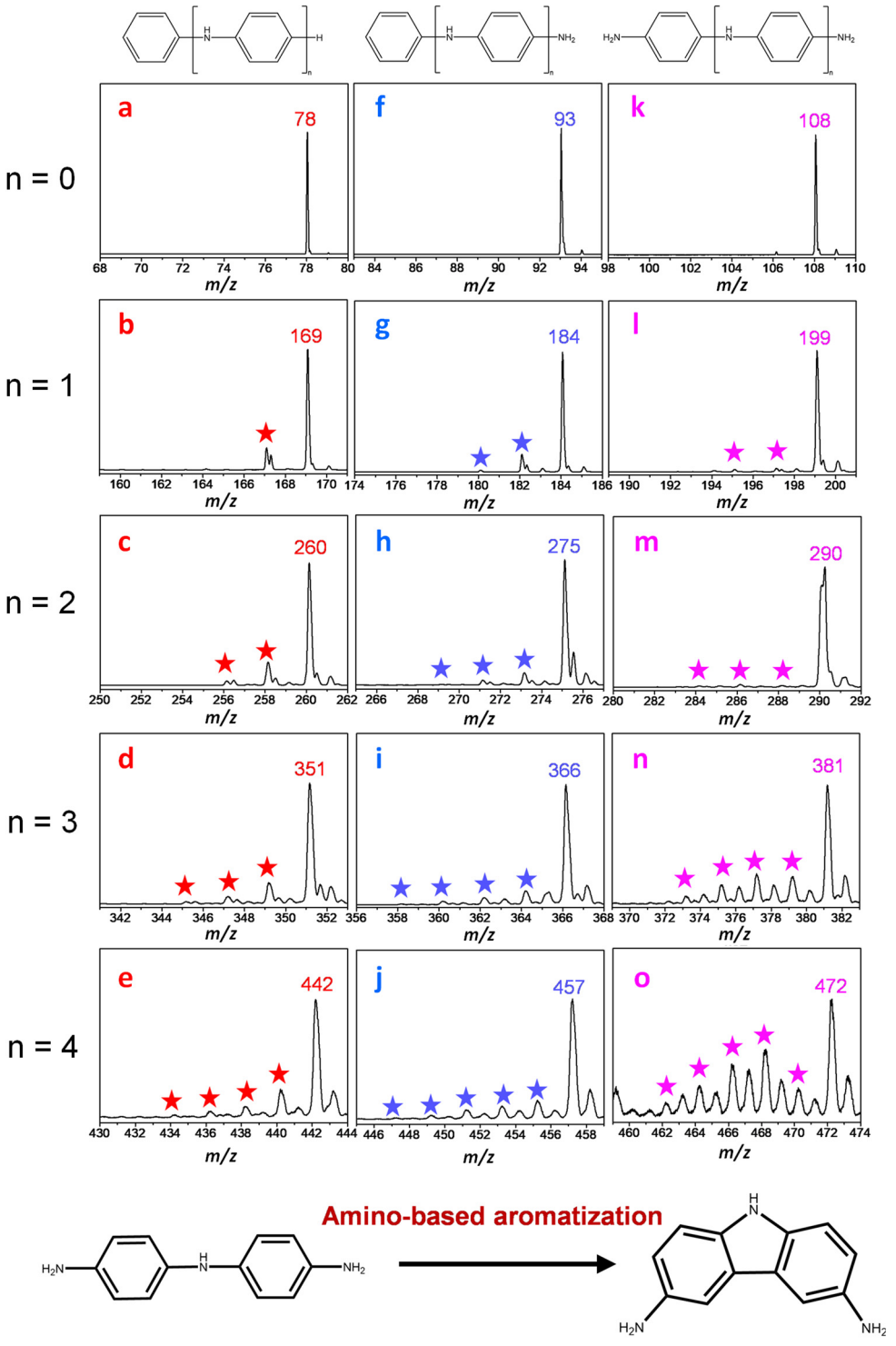

Figure 5. In situ Py-VUVPI-TOF MS spectra of polymer-I (**a**–**e**), polymer-II (**f**–**j**), and polymer-III (**k**–**o**). The star on the figure marks the process that the pyrolysis oligomer of polyaniline lasts for—2 Da.

The molecular mass information of the pyrolysis residue is shown in Figure 6. The molecular mass distribution of the pyrolysis residue is m/z 80–600. In the range of m/z 80–300, the species contained in the pyrolysis residue are almost completely different from the initial pyrolysis products. This phenomenon proves that the cyclic compounds in the initial pyrolysis products do not maintain a stable structure. In the range of m/z 300–600, aniline polymers and their derivatives with higher degrees of polymerization were retained.

In addition, compounds with a molecular mass interval of 1 appear continuously at m/z 300–600. This phenomenon indicates that the dearomatization reaction occurs during the pyrolysis process. Due to the complexity of polymer molecules, it is currently impossible to accurately determine the structural information of macromolecules. It is easier to infer accurate structures from mass spectrum peaks with a low mass distribution. Based on the general chemical formula and cyclization characteristics of the initial pyrolysis products, the structure of unique species (m/z = 80–300) in SE-LIAD-TOF MS characterization was speculated (Table S2). $C_{12}H_{10}N_2$, $C_{12}H_{18}N_2$, $C_{14}H_{10}N_2$, $C_{15}H_{11}N_3$, and $C_{16}H_{22}N_2$ can be derived from the initial pyrolysis products, which are mainly derived from the reaction between the initial pyrolysis products, H and NH radicals. The nitrogen in these compounds mainly exists in the form of pyrrole. The pyridine and pyrazine compounds were also detected in the pyrolysis residues, including monomers ($C_5H_{11}N$, $C_9H_{11}N$) and dimers ($C_{10}H_{10}N_2$, $C_9H_7N_3$). The six-membered heterocyclic structure of N is derived from the conversion of unstable intermediates in the initial products of pyrolysis. It is worth noting that a fused ring structure containing graphitic nitrogen functional groups (C_9H_6N and $C_9H_6N_4$) appeared in the pyrolysis residue. However, no compounds containing graphitic nitrogen structures were detected in the initial pyrolysis products.

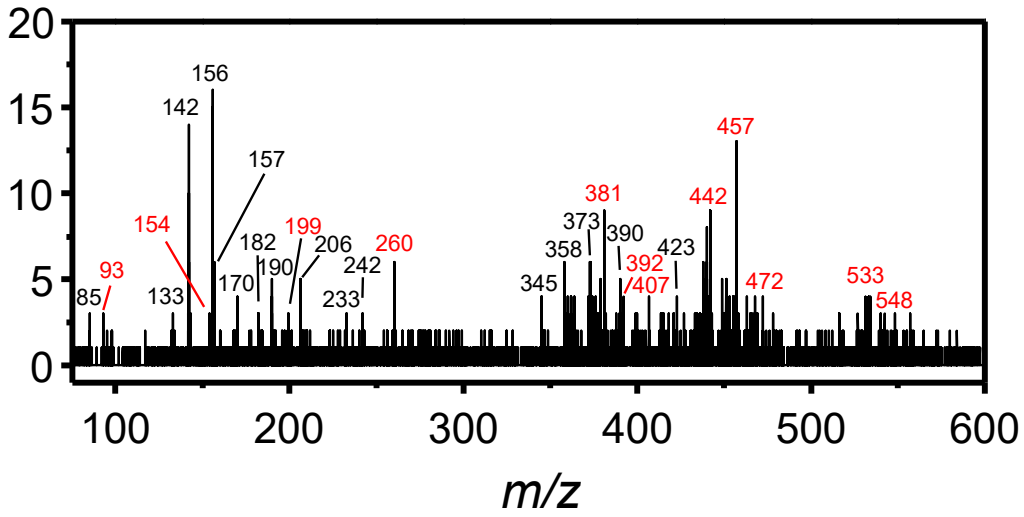

Figure 6. SE-LIAD-TOF MS spectra of pyrolysis residues on the focusing electrode (red mark: pyrolysis residues and initial co-owned products; black mark: unique products of pyrolysis residues).

The formation of graphitic nitrogen may come from the polymerization and conversion of precursors such as pyridine nitrogen and pyrrole nitrogen (carbazole) at high temperatures. This phenomenon is consistent with the conversion of nitrogen functional groups characterized by XPS [37]. The pyrolysis residues were analyzed by XPS, as shown in Figure 7, which proved the existence of graphitic nitrogen (blue line), pyrrole nitrogen (pink line), and pyridine nitrogen (green line). The generation of graphitic nitrogen at the edge is much easier than the replacement of carbon by nitrogen inside the carbon material, but this characteristic will also lead to an uneven distribution of nitrogen during the nitrogen doping process, and nitrogen functional groups are mainly abundant at the edge of the carbon material. An excessive local nitrogen doping concentration will lead to an unstable structure of carbon materials, which may be the main reason why the actual nitrogen doping amount of nitrogen-doped carbon materials is far lower than the theoretical doping amount [10]. The formation of graphitic nitrogen will inevitably cause the loss of the pyrrole nitrogen and pyridine nitrogen, resulting in the inability to obtain more edge pyridine nitrogen functional groups by simply controlling the temperature conditions.

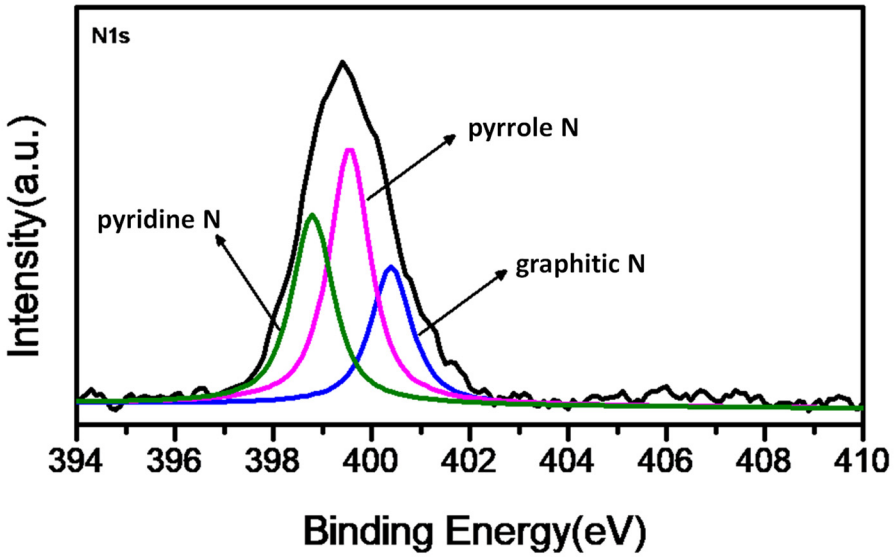

Figure 7. N1 XPS spectrum of the pyrolysis residue (black line). Blue line represents graphitic nitrogen (400.6 eV), pink line represents pyrrole nitrogen (399.5 eV), and green line represents pyridine nitrogen (398.6 eV).

3. Discussion

In previous reports, the process of nitrogen doping always occurred at the edges and the defects of carbon materials [5,16,38]. Both amino aromatization and free radical cyclization can realize the formation of pyrrole nitrogen and pyridine nitrogen at the edge. Compared with the free radical cyclization reaction, the amino-based aromatization reaction is more mild, which cannot be ignored in the formation of nitrogen-doped carbon materials. It is worth noting that the graphitic nitrogen functional groups cannot be detected in the initial pyrolysis products of PANI. In the XPS characterization of nitrogen-doped carbon materials, the content of graphitic nitrogen is similar to that of pyridine nitrogen and pyrrole nitrogen. The formation of graphitic nitrogen is probably not in the initial process of the nitrogen doping reaction.

Since the pyrolysis zone in in situ Py-VUVPI-TOF MS is under high vacuum (~10^{-4} Pa), the secondary reaction and condensation reaction are suppressed compared to the real situation. In addition, the distance between the pyrolysis product outlet and the ionization position is only ~10 mm, free radicals and intermediate products can be quickly ionized and detected (the process of pyrolysis parameters from desorption to ionization takes about tens to hundreds of microseconds). However, in situ pyrolysis provides the initial pyrolysis products, which are far from the final products. The process between the initial products and the final products is indispensable for understanding the pyrolysis reaction mechanism. In this work, SE-LIAD/TOF MS was used to detect pyrolysis residues as important supplements to pyrolysis information. The pyrolysis residues remain in the ion transmission system of the mass spectrometer through adsorption. In addition to the initial pyrolysis products, the pyrolysis residues also include the transitional pyrolysis products between the initial products and the final products. The pyrolysis residues represent the state of the initial pyrolysis products after a few microseconds. Since the temperature of the collecting electrode continues to remain below 100 °C, when the pyrolysis residue is adsorbed on the electrode, the thermal reaction of the pyrolysis residue will terminate and the pyrolysis product will evolve into a stable structure. In addition, this is the first report of SE-LIAD-TOF MS combined with in situ Py-VUVPI-TOF MS.

The formation of the nitrogen functional groups and intermolecular polymerization in the doping reaction mainly depends on free radical reactions (Figure 8). In the actual preparation process, the reaction conditions are in an inert atmosphere, and the collision probability between the molecules increases exponentially compared with that in vacuum.

Therefore, the process of preparing N-doped carbon materials (PANI, pyrrole, and NH_3 as nitrogen sources) generally requires a temperature of about 1000 °C. While achieving nitrogen doping, the high temperature treatment process will inevitably lead to the conversion of the existing form of nitrogen, such as the conversion of pyrrole nitrogen to pyridine nitrogen and graphitic nitrogen, and the conversion of pyridine nitrogen to graphitic nitrogen (Figure S8). During the pyrolysis process of PANI, the formation of almost all types of nitrogen-containing functional groups can be determined when the reaction temperature is below 500 °C. The path to form a nitrogen-containing heterocyclic ring by directly substituting a nitrogen atom for a carbon atom has not been detected. The formation of nitrogen-containing heterocycles mainly depends on the following paths: 1: Free radical cyclization reaction caused by aromatic ring cleavage; 2: amino-based aromatization reaction. Moreover, the path 2 reaction process does not involve the cleavage of C–C and C–N bonds. This is of great significance for the controllable synthesis of nitrogen functional groups in N-doped carbon materials. The nitrogen doping reaction occurring at the edge of the carbon materials can be achieved at a lower temperature, and it should also account for the majority of the nitrogen doping reaction. In the future design of nitrogen-doped catalysts, the way to provide more edge positions, such as surface defects and nitrogen sources, with suitable structures is the key to achieve increased nitrogen doping and controllable synthesis of nitrogen functional groups.

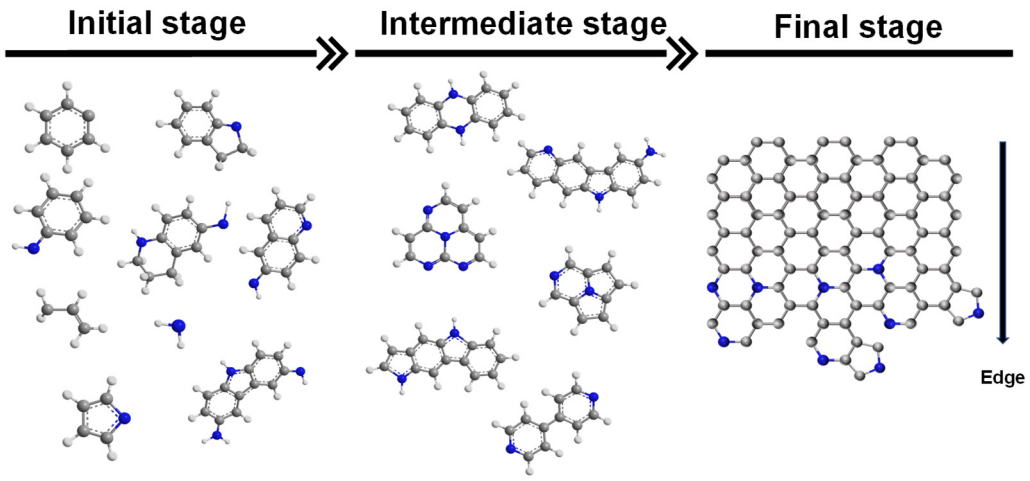

Figure 8. Nitrogen doping reaction process. The conversion process of pyrrole nitrogen to pyridine nitrogen and graphitic nitrogen, as well as the conversion of pyridine nitrogen to graphitic nitrogen, etc.

4. Materials and Methods

The experimental materials was PANI, with a purity > 98%, which was purchased from China Energy Chemical Co., Ltd. The structural formula of PANI is shown in Figure 9. The R group is mentioned above.

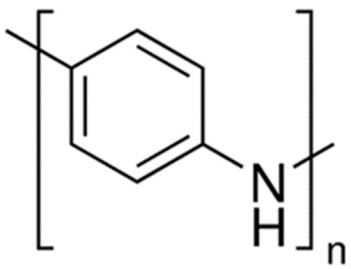

Figure 9. Polyaniline (PANI) structure.

The in situ pyrolysis process of polyaniline was investigated by in situ Py-VUVPI-TOF MS. The basic structure of in situ Py-VUVPI-TOF MS consists of two parts: a micro-heated pyrolyzer and a compact time-of-flight mass spectrometer (R~1500). The scheme of in situ Py-VUVPI-TOF MS is shown in Figure 10. Since the micro-heated pyrolyzer is under high vacuum, the secondary reaction of the initial pyrolysis products will be suppressed. At the same time, pyrolysis products only need to travel a distance of less than 10 mm, from the pyrolysis desorption to the complete ionization. Therefore, the secondary reaction in the pyrolysis process is effectively suppressed, and in situ Py-VUVPI-TOF MS can truly reflect the information of the initial pyrolysis products, such as free radicals and intermediates [29,39–44]. A vacuum ultraviolet light source generated by a vacuum ultraviolet lamp (Hamamatsu, L13301, with a light energy up to 10.78 eV, 8.5 W) was selected as the PI ionization source to achieve fragment-free detection [30]. In the pyrolysis experiment, 5–10 mg PANI was placed in a micro-heated pyrolyzer and heated from room temperature to 800 °C, at a heating rate of 10 °C/min. The detailed information of in situ Py-VUVPI-TOF MS has been described in previous works [28,29,39].

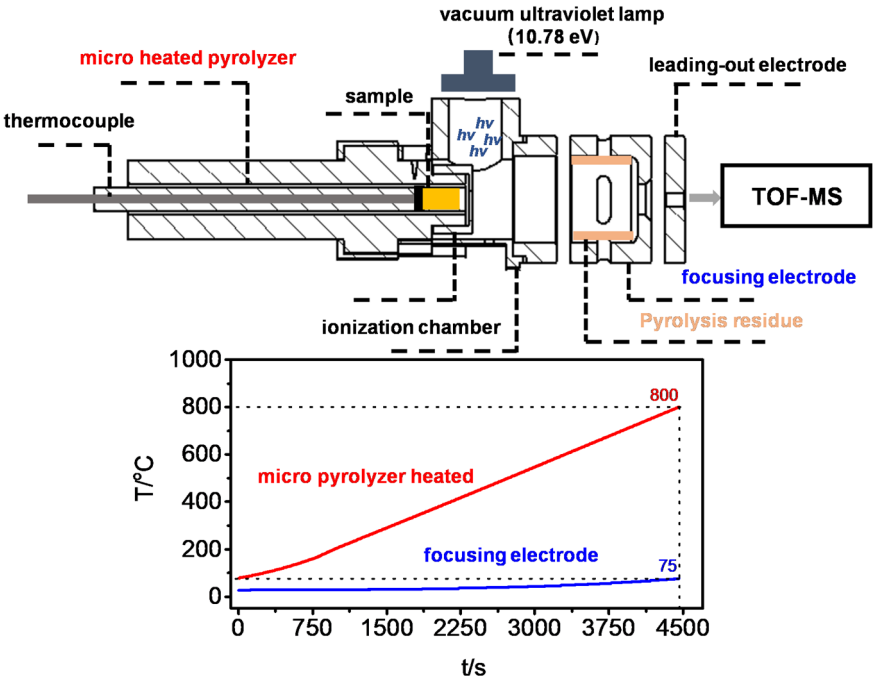

Figure 10. Schematic diagram of the in situ pyrolysis ion source, and the heating curve of the micro-heated pyrolyzer and focusing electrode.

Although in situ Py-VUVPI-TOF MS can obtain the initial pyrolysis products, it will inevitably ignore the subsequent reaction information of the initial pyrolysis products. It is worth noting that in the in situ pyrolysis experiment of in situ Py-VUVPI-TOF MS, the temperature of the focusing electrode is continuously kept below 80 °C due to the temperature isolation effect of the ceramic spacer (Figure 10). Thus, the low volatile substances in the pyrolysis products can be adsorbed on the focusing electrode. These pyrolysis residues can be regarded as the subsequent reaction products of the initial pyrolysis products, and their structure and composition information can reflect the intermediate process information between the initial pyrolysis products and the final pyrolysis products. However, the content of pyrolysis residues is extremely low. As an unknown complex analyte, its thermal stability and polarity are unknown. Traditional analytical methods, such as MALDI-MS and GC-MS, cannot fully reflect the composition information of the pyrolysis residues. Compared with traditional mass spectrometry methods, SE-LIAD-TOF MS has the characteristics of high sensitivity, mild desorption, and single-photon ionization, without polarity discrimination, making it suitable for the analysis of pyrolysis residues. LIAD can mildly

desorb the analyte loaded on the other side into the gas phase through the ultrasound generated by the laser irradiation on the metal foil. By combining this with single-photon ionization, a high sensitivity and fragment-free detection of analytes can be achieved. In the experiment, acetone was used as a solvent to dissolve the pyrolysis residues attached to the focusing electrode after in situ pyrolysis of polyaniline, which was evenly coated on the surface of titanium foil and then placed in an oven for evaporation and drying. Finally, the analyte on the surface of the titanium foil was detected by SE-LIAD-TOF MS. The detailed information and analysis process of SE-LIAD-TOF MS have been described in a previous work [30].

All quantum chemical calculations were implemented with a Gaussian 16 program [45]. The density functional theory method, B3LYP and 6-31G(d) basis set, were used to calculate the bond order information of PANI and the spatial structure of pyrolysis product isomers.

5. Conclusions

In this work, the pyrolysis process (10 °C/min, room temperature −800 °C) of PANI, as a model reaction of N-doped carbon materials, was investigated at a molecular level through in situ Py-VUVPI-TOF MS and SE-LIAD-TOF MS. The initial pyrolysis process of PANI is mainly composed of three basic reactions: 1. the cleavage of C–N bond mainly produces aniline monomer and its polymers; 2. the cleavage of the aromatic ring (C–C bond cleavage) mainly produces small molecule hydrocarbons and nitrogen-containing heterocycles; 3. the amino-based aromatization reaction mainly produces carbazole structure. Nitrogen-containing heterocyclic compounds mainly appear in the form of pyrrole nitrogen and pyridine nitrogen in the initial pyrolysis products. Graphitic nitrogen does not appear in the initial stage of the pyrolysis reaction, it is mainly formed by the addition reaction of the initial pyrolysis reaction products. The nitrogen doping reaction at the edge is the main reaction in the nitrogen doping process. It is necessary to design carbon sources with more reaction sites (such as vacancy) to achieve a higher doping amount. Moreover, because of the complexity of the nitrogen doping reaction at high temperatures, obtaining the required free radicals at low temperatures is an ideal approach to control the synthesis of nitrogen functional groups. Since the amino aromatization reaction does not involve the dissociation of the aromatic ring, it may be an effective idea for the design of N-doped carbon materials in the future.

Supplementary Materials: The following supporting information can be downloaded at: https://www.mdpi.com/article/10.3390/catal13050830/s1, Figure S1: In situ Py-PI-TOF MS spectra of the in situ pyrolysis of PANI (a) ×1, (b) ×100. Figure S2: In situ Py-PI-TOF MS spectra of the in situ pyrolysis of PANI (partial enlarged detail). Figure S3: Bond order information of PANI (aniline tetramer): blue represents N, gray represents C, and white represents H. Figure S4: Ion current of N-cycle-I n = 0 (a), n = 1 (b), n = 2 (c), n = 3 (d). Figure S5: Ion current of N-cycle-I (a), N-cycle-II (b), N-cycle-III (c), and N-cycle-IV (d) (n = 0). Figure S6: Ion current of polymer-I and its cyclization products, (a) n = 1, (b) n = 2, (c) n = 3, (d) n = 4. Figure S7: Possible isomers of nitrogen-containing heterocyclic compounds (N-cycle-I, N-cycle-II, N-cycle-III, and N-cycle-IV). Figure S8: Visualization of the evolution of nitrogen functionalities in carbonaceous materials during pyrolysis; Table S1: The main initial pyrolysis products of PANI (by in situ Py-PI-TOF MS). Table S2: Unique products of the pyrolysis residue in m/z 0–300.

Author Contributions: Y.J.: conceptualization, methodology, investigation, formal analysis, data curation, writing—original draft, validation, visualization. Z.S.: conceptualization, methodology, data curation, writing—original draft, validation, visualization. Q.Z.: conceptualization, methodology, formal analysis. J.Z.: investigation, data curation, visualization. Z.D. and J.Y. (Jing Yang): visualization. Q.W.: resources. J.Y. (Jingxiong Yu): conceptualization, resources, methodology, investigation, supervision, project administration, validation, visualization, writing—review and editing. Z.Q. and Z.T.: resources, conceptualization, methodology, supervision, project administration. All authors have read and agreed to the published version of the manuscript.

Funding: This research was supported by the National Key Research and Development Program of China (2016YFB0600301), the National Science Foundation of China (21873003,91961107), and the

National Natural Science Foundation of China Youth Science Fund (21805231). This work is also supported by the University Cooperation and Innovation Program of Anhui (GXXT-2020-004) and the Open Foundation of Key Laboratory of High Power Laser and Physics, Chinese Academy of Sciences (SGKF202106).

Data Availability Statement: Data will be made available on request.

Conflicts of Interest: The authors declare no conflict of interest.

References

1. Morozan, A.; Jousselme, B.; Palacin, S. Low-platinum and platinum-free catalysts for the oxygen reduction reaction at fuel cell cathodes. *Energy Environ. Sci.* **2011**, *4*, 1238–1254. [CrossRef]
2. Gasteiger, H.A.; Panels, J.E.; Yan, S.G. Dependence of PEM fuel cell performance on catalyst loading. *J. Power Sources* **2004**, *127*, 162–171. [CrossRef]
3. Silva, R.; Voiry, D.; Chhowalla, M.; Asefa, T. Efficient metal-free electrocatalysts for oxygen reduction: Polyaniline-derived N- and O-doped mesoporous carbons. *J. Am. Chem. Soc.* **2013**, *135*, 7823–7826. [CrossRef]
4. Qu, L.T.; Liu, Y.; Baek, J.B.; Dai, L.M. Nitrogen-Doped Graphene as Efficient Metal-Free Electrocatalyst for Oxygen Reduction in Fuel Cells. *ACS Nano* **2010**, *4*, 1321–1326. [CrossRef]
5. Lv, Q.; Si, W.Y.; He, J.J.; Sun, L.; Zhang, C.F.; Wang, N.; Yang, Z.; Li, X.D.; Wang, X.; Deng, W.Q.; et al. Selectively nitrogen-doped carbon materials as superior metal-free catalysts for oxygen reduction. *Nat. Commun.* **2018**, *9*, 3376. [CrossRef]
6. Inagaki, M.; Toyoda, M.; Soneda, Y.; Morishita, T. Nitrogen-doped carbon materials. *Carbon* **2018**, *132*, 104–140. [CrossRef]
7. Singh, S.K.; Takeyasu, K.; Nakamura, J. Active sites and mechanism of oxygen reduction reaction electrocatalysis on nitrogen-doped carbon materials. *Adv. Mater.* **2019**, *31*, 1804297. [CrossRef]
8. Liu, S.; Yang, H.B.; Huang, X.; Liu, L.H.; Cai, W.Z.; Gao, J.J.; Li, X.N.; Zhang, T.; Huang, Y.Q.; Liu, B. Identifying active sites of nitrogen-doped carbon materials for the CO_2 reduction reaction. *Adv. Funct. Mater.* **2018**, *28*, 1800499. [CrossRef]
9. Park, M.; Ryu, J.; Kim, Y.; Cho, J. Corn protein-derived nitrogen-doped carbon materials with oxygen-rich functional groups: A highly efficient electrocatalyst for all-vanadium redox flow batteries. *Energy Environ. Sci.* **2014**, *7*, 3727–3735. [CrossRef]
10. Shi, Z.M.; Kutana, A.; Yakobson, B.I. How much N-doping can graphene sustain? *J. Phys. Chem. Lett.* **2015**, *6*, 106–112. [CrossRef]
11. Salinas-Torres, D.; Shiraishi, S.; Morallon, E.; Cazorla-Amoros, D. Improvement of carbon materials performance by nitrogen functional groups in electrochemical capacitors in organic electrolyte at severe conditions. *Carbon* **2015**, *82*, 205–213. [CrossRef]
12. Frackowiak, E.; Lota, G.; Machnikowski, J.; Vix-Guterl, C.; Beguin, F. Optimisation of supercapacitors using carbons with controlled nanotexture and nitrogen content. *Electrochim. Acta* **2006**, *51*, 2209–2214. [CrossRef]
13. Lota, G.; Grzyb, B.; Machnikowska, H.; Machnikowski, J.; Frackowiak, E. Effect of nitrogen in carbon electrode on the supercapacitor performance. *Chem. Phys. Lett.* **2005**, *404*, 53–58. [CrossRef]
14. Ornelas, O.; Sieben, J.M.; Ruiz-Rosas, R.; Morallon, E.; Cazorla-Amoros, D.; Geng, J.; Soin, N.; Siores, E.; Johnson, B.F.G. On the origin of the high capacitance of nitrogen-containing carbon nanotubes in acidic and alkaline electrolytes. *Chem. Commun.* **2014**, *50*, 11343–11346. [CrossRef] [PubMed]
15. Zhang, C.Z.; Hao, R.; Liao, H.B.; Hou, Y.L. Synthesis of amino-functionalized graphene as metal-free catalyst and exploration of the roles of various nitrogen states in oxygen reduction reaction. *Nano Energy* **2013**, *2*, 88–97. [CrossRef]
16. Guo, D.H.; Shibuya, R.; Akiba, C.; Saji, S.; Kondo, T.; Nakamura, J. Active sites of nitrogen-doped carbon materials for oxygen reduction reaction clarified using model catalysts. *Science* **2016**, *351*, 361–365. [CrossRef]
17. Nam, G.; Park, J.; Kim, S.T.; Shin, D.B.; Park, N.; Kim, Y.; Lee, J.S.; Cho, J. Metal-free ketjenblack incorporated nitrogen-doped carbon sheets derived from gelatin as oxygen reduction catalysts. *Nano Lett.* **2014**, *14*, 1870–1876. [CrossRef]
18. Daems, N.; Sheng, X.; Vankelecom, I.F.J.; Pescarmona, P.P. Metal-free doped carbon materials as electrocatalysts for the oxygen reduction reaction. *J. Mater. Chem. A* **2014**, *2*, 4085–4110. [CrossRef]
19. Lin, Y.C.; Teng, P.Y.; Yeh, C.H.; Koshino, M.; Chiu, P.W.; Suenaga, K. Structural and chemical dynamics of pyridinic-nitrogen defects in graphene. *Nano Lett.* **2015**, *15*, 7408–7413. [CrossRef]
20. Xu, B.; Hou, S.S.; Cao, G.P.; Wu, F.; Yang, Y.S. Sustainable nitrogen-doped porous carbon with high surface areas prepared from gelatin for supercapacitors. *J. Mater. Chem.* **2012**, *22*, 19088–19093. [CrossRef]
21. Nakajima, T.; Koh, M.; Katsube, T. Structure, chemical bonding and electrochemical behavior of heteroatom-substituted carbons prepared by arc discharge and chemical vapor deposition. *Solid State Sci.* **2000**, *2*, 17–29. [CrossRef]
22. Liu, J.; Song, P.; Xu, W.L. Structure-activity relationship of doped-nitrogen (N)-based metal-free active sites on carbon for oxygen reduction reaction. *Carbon* **2017**, *115*, 763–772. [CrossRef]
23. Li, L.; Zhou, G.M.; Yin, L.C.; Koratkar, N.; Li, F.; Cheng, H.M. Stabilizing sulfur cathodes using nitrogen-doped graphene as a chemical immobilizer for Li-S batteries. *Carbon* **2016**, *108*, 120–126. [CrossRef]
24. Schiros, T.; Nordlund, D.; Palova, L.; Prezzi, D.; Zhao, L.Y.; Kim, K.S.; Wurstbauer, U.; Gutierrez, C.; Delongchamp, D.; Jaye, C.; et al. Connecting dopant bond type with electronic structure in N-doped graphene. *Nano Lett.* **2012**, *12*, 4025–4031. [CrossRef] [PubMed]
25. Quilez-Bermejo, J.; Morallon, E.; Cazorla-Amoros, D. Oxygen-reduction catalysis of N-doped carbons prepared via heat treatment of polyaniline at over 1100 degrees C. *Chem. Commun.* **2018**, *54*, 4441–4444. [CrossRef]

26. Zhu, B.Y.; Deng, Z.; Yang, W.L.; Wang, H.B.; Gao, L.J. Pyrolyzed polyaniline and graphene nano sheet composite with improved rate and cycle performance for lithium storage. *Carbon* **2015**, *92*, 354–361. [CrossRef]
27. Xiao, H.; Xie, P.; Qiu, S.J.; Rong, M.Z.; Zhang, M.Q. Ultrathin-graphite foam with high mechanical resilience and electroconductibility fabricated through morphology-controlled solid-state pyrolysis of polyaniline foam. *Carbon* **2018**, *139*, 648–655. [CrossRef]
28. Zhou, Y.; Li, L.; Jin, L.J.; Zhou, J.; Shi, Z.W.; Li, Y.; Hu, H.Q. Pyrolytic behavior of coal-related model compounds connected with C-C bridged linkages by in-situ pyrolysis vacuum ultraviolet photoionization mass spectrometry. *Fuel* **2019**, *241*, 533–541. [CrossRef]
29. Shi, L.; Wang, X.L.; Zhang, S.Y.; Wu, X.H.; Yuan, L.; Tang, Z.C. A new in-situ pyrolytic time-of-flight mass spectrometer instrument for study on coal pyrolysis. *J. Anal. Appl. Pyrolysis* **2016**, *117*, 347–353. [CrossRef]
30. Yu, J.X.; Chen, Y.W.; Zhang, J.L.; Chen, S.J.; Wang, Q.L.; Qin, Z.B.; Tang, Z.C. Development of a miniature time-of-flight mass spectrometer coupled with an improved substrate-enhanced laser-induced acoustic desorption source (SE-LIAD/TOF-MS). *Analyst* **2021**, *146*, 4365–4373. [CrossRef]
31. Dibeler, V.H.; Walker, J.A.; Rosenstock, H.M. Mass spectrometric study of photoionization V. water and ammonia. *J. Res. Natl. Bur. Stand. Sect. A Phys. Chem.* **1966**, *70A*, 459–463. [CrossRef]
32. Dunlavey, S.J.; Dyke, J.M.; Jonathan, N.; Morris, A. Vacuum ultraviolet photoelectron-spectroscopy of transient species. 11. NH2(X2B1) radical. *Mol. Phys.* **1980**, *39*, 1121–1135. [CrossRef]
33. de Castro, D.G.; Poveda, L.A.; Crispim, L.W.S.; Ballester, M.Y. Quasi-Classical Trajectory Study of NH((3) summation operator(-)) + NH((3) summation operator(-)) Reactive Collisions. *J. Phys. Chem. A* **2019**, *123*, 9113–9122. [CrossRef] [PubMed]
34. Ponomarev, D.; Takhistov, V. Some regularities in the relative thermodynamic stabilities of free radicals. *J. Mol. Struct.* **1997**, *435*, 259–274. [CrossRef]
35. Rohrig, M.; Wagner, H.G. A kinetic-study about the reactions of NH(x3-sigma-) with hydrocarbons. 1. saturated-hydrocarbons and acetaldehyde. *Ber. Bunsen Ges. Phys. Chem. Chem. Phys.* **1994**, *98*, 858–863. [CrossRef]
36. Wang, W.D.; Lin, X.Q.; Zhao, H.B.; Lu, Q.F. Nitrogen-doped graphene prepared by pyrolysis of graphene oxide/polyaniline composites as supercapacitor electrodes. *J. Anal. Appl. Pyrol.* **2016**, *120*, 27–36. [CrossRef]
37. Pels, J.R.; Kapteijn, F.; Moulijn, J.A.; Zhu, Q.; Thomas, K.M. Evolution of nitrogen functionalities in carbonaceous materials during pyrolysis. *Carbon* **1995**, *33*, 1641–1653. [CrossRef]
38. Dai, L.M.; Xue, Y.H.; Qu, L.T.; Choi, H.J.; Baek, J.B. Metal-free catalysts for oxygen reduction reaction. *Chem. Rev.* **2015**, *115*, 4823–4892. [CrossRef]
39. Li, G.; Zhang, S.Y.; Jin, L.J.; Tang, Z.C.; Hu, H.Q. In-situ analysis of volatile products from lignite pyrolysis with pyrolysis-vacuum ultraviolet photoionization and electron impact mass spectrometry. *Fuel Process. Technol.* **2015**, *133*, 232–236. [CrossRef]
40. Guo, X.G.; Fang, G.Z.; Li, G.; Ma, H.; Fan, H.J.; Yu, L.; Ma, C.; Wu, X.; Deng, D.H.; Wei, M.M.; et al. Direct, nonoxidative conversion of methane to ethylene, aromatics, and hydrogen. *Science* **2014**, *344*, 616–619. [CrossRef]
41. Shi, Z.; Jin, L.; Zhou, Y.; Li, H.; Li, Y.; Hu, H. In-situ analysis of catalytic pyrolysis of Baiyinhua coal with pyrolysis time-of-flight mass spectrometry. *Fuel* **2018**, *227*, 386–393. [CrossRef]
42. Wang, T.; Tang, X.-F.; Wen, Z.-Y.; Zhang, C.-H.; Zhang, W.-J. A Vacuum Ultraviolet Photoionization Time-of-Flight Mass Spectrometer for Investigation of Free Radical Reaction. *Chin. J. Anal. Chem.* **2020**, *48*, 28–33. [CrossRef]
43. Shao, K.; Liu, X.; Jones, P.J.; Sun, G.; Gomez, M.; Riser, B.P.; Zhang, J. Thermal decomposition of cyclohexane by flash pyrolysis vacuum ultraviolet photoionization time-of-flight mass spectrometry: A study on the initial unimolecular decomposition mechanism. *Phys. Chem. Chem. Phys.* **2021**, *23*, 9804–9813. [CrossRef]
44. Shi, Z.; Jiang, Y.; Yu, J.; Chen, S.; Chen, J.; Tang, Z.; Zheng, L. Developing the Low-Temperature Oxidation Mechanism of Cyclopentane: An Experimental and Theoretical Study. *Chem. A Eur. J.* **2022**, *28*, e202103546. [CrossRef]
45. Frisch, M.J.; Trucks, G.W.; Schlegel, H.B.; Scuseria, G.E.; Robb, M.A.; Cheeseman, J.R.; Scalmani, G.; Barone, V.; Petersson, G.A.; Nakatsuji, H.; et al. *Gaussian 16 Revision C.01*; Gaussian Inc.: Wallingford, CT, USA, 2016.